Engineering Optimization
Publication details, including instructions for authors and subscription information:
http://www.tandfonline.com/loi/geno20

Multi-objective robust design of energy-absorbing components using coupled process-performance simulations

Ali Najafi[a], Erdem Acar[b] & Masoud Rais-Rohani[a]

[a] Department of Aerospace Engineering and Center for Advanced Vehicular Systems, Mississippi State University, Mississippi, MS 39762, USA

[b] Department of Mechanical Engineering, TOBB University of Economics and Technology, Söğütözü, Ankara, Turkey

Published online: 26 Feb 2013.

To cite this article: Ali Najafi, Erdem Acar & Masoud Rais-Rohani (2014) Multi-objective robust design of energy-absorbing components using coupled process-performance simulations, Engineering Optimization, 46:2, 146-164, DOI: 10.1080/0305215X.2012.753437

To link to this article: http://dx.doi.org/10.1080/0305215X.2012.753437

Engineering Optimization, 2014
Vol. 46, No. 2, 146–164, http://dx.doi.org/10.1080/0305215X.2012.753437

Taylor & Francis
Taylor & Francis Group

Multi-objective robust design of energy-absorbing components using coupled process–performance simulations

Ali Najafi[a], Erdem Acar[b] and Masoud Rais-Rohani[a]*

[a]*Department of Aerospace Engineering and Center for Advanced Vehicular Systems, Mississippi State University, Mississippi, MS 39762, USA;* [b]*Department of Mechanical Engineering, TOBB University of Economics and Technology, Söğütözü, Ankara, Turkey*

(*Received 11 March 2012; final version received 5 November 2012*)

The stochastic uncertainties associated with the material, process and product are represented and propagated to process and performance responses. A finite element-based sequential coupled process–performance framework is used to simulate the forming and energy absorption responses of a thin-walled tube in a manner that both material properties and component geometry can evolve from one stage to the next for better prediction of the structural performance measures. Metamodelling techniques are used to develop surrogate models for manufacturing and performance responses. One set of metamodels relates the responses to the random variables whereas the other relates the mean and standard deviation of the responses to the selected design variables. A multi-objective robust design optimization problem is formulated and solved to illustrate the methodology and the influence of uncertainties on manufacturability and energy absorption of a metallic double-hat tube. The results are compared with those of deterministic and augmented robust optimization problems.

Keywords: metal forming simulation; crash simulation; process–performance simulation; robust design optimization

1. Introduction

Traditionally, the effects of manufacturing process on the component geometry and material microstructure/state are ignored. However, studies show that these effects can influence the overall behaviour of a structural component (Oliveira *et al.* 2006; Najafi, Marin, and Rais-Rohani, 2012). One way to address this concern is to perform sequential coupled process–performance simulations whereby both material properties and component geometry can evolve from one stage to the next for a more accurate prediction of the structural performance measures (Najafi, Rais-Rohani, and Hammi 2011). Therefore, the characterization tests are performed on the stock material and the evolution of material microstructure is tracked by mapping the material state variables from manufacturing to performance simulation.

Previous studies on coupled process–performance simulations have considered components made of different materials such as aluminium (Kaufman *et al.* 1998; Gholipour, Worswick, and Oliveira 2004; Williams *et al.* 2005), steel (Dutton *et al.* 2001; Simunovic, Shaw, and Aramayo 2001; Simunovic and Aramayo 2002) and magnesium (Najafi, Rais-Rohani, and Hammi

*Corresponding author. Email: Masoud@ae.msstate.edu

2011; Najafi and Rais-Rohani 2012) alloys in different crush tube geometries. Both experimental (Grantab 2006) and computational studies have shown that the manufacturing process can affect the energy absorption behaviour of crush tubes. The main material history effect considered in these studies is the plastic strain in each element that updates the original yield point of the material.

Recently, Najafi and Rais-Rohani (2012) performed sequential coupled process–performance simulation and multi-objective optimization of thin-walled tubes. However, that study did not consider the presence or the effect of uncertainties associated with the manufacturing process. As an extension of that research, this article examines the representation of uncertainties associated with the geometric size of the forming tools, blank thickness and material properties, and their propagation to both manufacturing responses and crush behaviour. A robust optimization technique is used to optimize the process–performance design optimization in the presence of uncertainties.

Since forming, springback and crush simulations are computationally expensive, surrogate models are developed prior to solving the selected optimization problems. Two different sets of metamodels are constructed. The first set relates the responses to the random variables and is used within a Monte Carlo framework to compute the means and standard deviations of the responses, whereas the second set relates the means and the standard deviations of the responses to the design variables. The second set of metamodels is used within a multi-objective genetic algorithm framework to solve the coupled process–product design optimization problems under uncertainty.

2. Coupled simulations

A sequential coupled process–performance simulation framework was recently developed (Najafi and Rais-Rohani 2012) with Abaqus/Explicit (version 6.10) for the deep drawing analysis, Abaqus/Standard (version 6.10) for the springback analysis under isothermal condition, followed by Abaqus/Explicit simulation for the crush analysis. Figure 1 illustrates the sequential coupled simulation approach for a double-hat tube modelled by forming and joining two identical single-hat sections that form a symmetric cross-section.

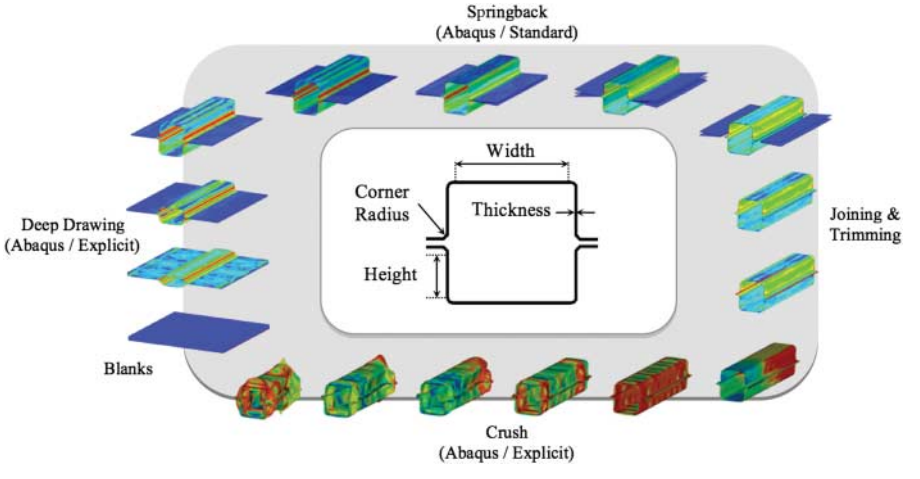

Figure 1. Coupled process–performance simulations of the double-hat crush tube.

In the forming simulation, the contact surfaces are defined using the penalty formulation with the friction coefficient serving as a manufacturing process parameter for an equivalent representation of both surface roughness and draw beads. Punch velocity is held constant in this analysis. Rupture and thinning are the two manufacturability responses of interest in the sheet-forming process.

Rupture is calculated by comparing the principal major and minor plastic strains in each finite element with the forming limit diagram (FLD) (Lee *et al.* 2008). The overall measure of the rupture response is calculated as:

$$R = \begin{cases} \sum_{i=1}^{n} R_i^2 = \sum_{i=1}^{n} (\varepsilon_1^i - \phi(\varepsilon_2^i))^2 & \varepsilon_1^i > \phi(\varepsilon_2^i) \\ 0 & \varepsilon_1^i \leq \phi(\varepsilon_2^i) \end{cases} \tag{1}$$

where $\phi(\varepsilon_2^i)$ is the equation representing the FLD curve with ε_1^i and ε_2^i as the principal major and minor strains, respectively, at each integration point through the thickness. Parameter n represents the total number of elements.

The overall measure of thinning is calculated as:

$$T = \sum_{i=1}^{n} T_i^2 = \sum_{i=1}^{n} \left(\frac{t_i - t_o}{t_o} \right)^2 \tag{2}$$

where t_o and t_i are the initial (blank) and final (component) shell thicknesses, respectively.

Once the deep-drawing operation is completed and the tools are removed, the formed part will have a tendency to change its geometry in what is commonly called springback. The springback analysis is performed by considering the component geometry from the deep drawing simulation together with the accompanying residual stresses, effect of the contact condition and the dynamic effects of deep drawing. A single springback metric is defined in terms of deviation angle as:

$$S = \frac{\text{Max}(\sqrt{(X_i - X_o)^2 + (Y_i - Y_o)^2 + (Z_i - Z_o)^2})}{H} \tag{3}$$

where X, Y and Z are the nodal coordinates, with subscripts i and o representing the values at the beginning and the end of springback simulation, respectively, and H represents the height of a single hat section.

Following the manufacturing process simulations, the two hat sections are joined together assuming a perfect connection with the excess tabs trimmed as shown in Figure 1. The flanges are joined using bond contact formulation. Component mass, M, is found by adding the contributions of all the elements in the tube model at their respective post-forming thickness values.

For crush simulation, the multicorner tube is held fixed at one end while it is loaded at the other end by a rigid wall moving at a constant velocity. The tube's initial state in this simulation is defined based on the outputs of the previous simulations. The maximum crush force, $P_{\max}$, is calculated from the contact force history of the rigid wall during the crush simulation while the mean crush force is derived as (Najafi and Rais-Rohani 2011):

$$P_{\text{m}} = \frac{1}{\delta_{\text{eff}}} \int_0^t F(t) D(t) \, \text{d}t \tag{4}$$

where $F(t)$ is the instantaneous contact force, $D(t)$ is the axial displacement of the rigid wall, and the effective crush distance is set at $\delta_{\text{eff}} = 125$ mm or half the tube length.

The material is modelled as bi-linear elastic–plastic with isotropic hardening. Rate dependency is ignored in this study to reduce the computational complexity. The nominal values are taken to be approximately those for AZ31 magnesium alloy sheet, with elastic modulus = 45 GPa, tangent modulus = 21 GPa, yield stress = 150 MPa, Poisson's ratio = 0.33 and density = 1.738 kg/m^3.

3. Design optimization problems

With the goal of minimizing the sensitivity of the tube design to the manufacturing-induced uncertainties, a multi-objective robust design optimization problem is formulated as:

$$\begin{aligned} \text{Find} \quad & \mathbf{x} \\ \text{Min} \quad & \{\text{Var}(R), \text{Var}(T), \text{Var}(S), \text{Var}(P_{\text{m}}), \text{Var}(P_{\max}), \text{Var}(M)\} \\ \text{s.t.} \quad & \mathbf{x}^{\text{L}} \leq \mathbf{x} \leq \mathbf{x}^{\text{U}} \end{aligned} \tag{5}$$

where x represents the vector of design variables and Var(.) is the variance of the designated random process or performance response. The lower and the upper bounds for the design variables are denoted by x^{L} and x^{U}, respectively. The mean values of seven random variables that control the manufacturing process and the tube geometry (Figure 1) are used as the design variables with bounds defined in Table 2 (see below).

Table 1 shows, in three separate groups, 12 random variables and the corresponding mean and standard deviation (SD) values. All the random variables are assumed to follow a truncated normal distribution. FLD-*a* and FLD-*b* denote the coefficients (slope and intercept) of a linear equation describing the lower boundary of FLD (Hu, Yao, and Hua, 2008; Wei and Yuying 2008).

A deterministic variant of Equation (5) with all the uncertainties ignored is also considered, where the variance terms are replaced by the mean values of the designated responses as:

$$\begin{aligned} \text{Find} \quad & \mathbf{x} \\ \text{Min} \quad & \{\bar{R}, \bar{T}, \bar{S}, -\bar{P}_{\text{m}}, \bar{P}_{\max}, \bar{M}\} \\ \text{s.t.} \quad & \mathbf{x}^{\text{L}} \leq \mathbf{x} \leq \mathbf{x}^{\text{U}} \end{aligned} \tag{6}$$

The combination of the previous two optimization problems is also considered. The so-called augmented robust design problem is formulated as:

$$\begin{aligned} \text{Find} \quad & \mathbf{x} \\ \text{Min} \quad & \{\bar{R}, \bar{T}, \bar{S}, -\bar{P}_{\text{m}}, \bar{P}_{\max}, \bar{M}, \text{Var}(R), \text{Var}(T), \text{Var}(S), \text{Var}(P_{\text{m}}), \text{Var}(P_{\max}), \text{Var}(M)\} \\ \text{s.t.} \quad & \mathbf{x}^{\text{L}} \leq \mathbf{x} \leq \mathbf{x}^{\text{U}} \end{aligned} \tag{7}$$

Equations (5)–(7) are solved following the determination of accurate global response surface models as discussed in the next section.

Table 1. The random variables and associated statistical properties.

Group	Random variable	Mean	SD
Product	Width (mm)	55	0.55
	Height (mm)	27.5	0.275
	Corner radius (mm)	6	0.30
	Blank thickness (mm)	2	0.06
Process	Holding force (kN)	30	0.75
	Punch velocity (m/s)	6	0.3
	Friction coefficient	0.225	0.0405
	FLD-*a*	0.7579	0.038
	FLD-*b*	0.007	0.00021
Material	Young's modulus (GPa)	45	1.35
	Yield stress (MPa)	150	12
	Tangent modulus (GPa)	21	0.63

4. Response approximation

Although direct integration of metal forming and crush simulations is possible, it is computationally prohibitive within an optimization framework as numerous simulations would be required. To alleviate the computational burden, metamodelling techniques are used.

Two different sets of metamodels are developed. The first set, called analysis metamodels (AMMs), is constructed to relate the responses to the random variables. The AMMs are used within a Monte Carlo framework to compute the mean and the standard deviation values of the corresponding responses. The second set of metamodels, called design metamodels (DMMs), is generated to relate the mean and the standard deviation values of the responses to the design variables. The terminology of 'analysis metamodel' and 'design metamodel' is borrowed from the work of Qu *et al.* (2003).

The metamodelling techniques considered include polynomial response surface approximations (PRS) (Myers and Montgomery 2002), stepwise regression (SWR) (Myers and Montgomery 2002), radial basis functions, RBF (Buhmann 2003, Mullur and Messac 2005), kriging (KR) (Sacks *et al.* 1989; Martin and Simpson 2005) and the optimized ensemble of metamodels (ENS) (Acar and Rais-Rohani 2008).

The specific metamodels used here include linear PRS and SWR (PRS1 and SWR1), quadratic PRS and SWR (PRS2 and SWR2), multiquadric RBF (RBFM), inverse multiquadric RBF (RBFI), KR with Gaussian correlation plus constant trend (KR0) and linear trend (KR1), as well as ENS representing a weighted average of the aforementioned eight models (*i.e.* PRS1, SWR1, PRS2, SWR2, RBFM, RBFI, KR0 and KR1). The weight factors in ENS are selected such that the root mean square of the leave-one-out cross-validation error is minimized.

4.1. *Analysis metamodels*

To develop the AMMs, 120 training points (10 times the number of random variables in Table 1) are generated using the Latin hypercube sampling (LHS) technique. The sampling bounds for the first six random variables are taken as the lower bounds in Table 2 minus three standard deviations and the upper bounds in Table 2 plus three standard deviations, whereas for the friction coefficient, plus or minus two standard deviations are used to preserve positive values. The sampling bounds for the other five random variables are taken as the mean plus and minus three standard deviations. In addition to the training points, 20 independent test points are generated using LHS for metamodel accuracy assessment. The minimum and the maximum values of the responses at the training and test points in the random space are provided in Table 3. The symbols introduced in Equations (1)–(4) are used to identify the responses in column 1 of Table 3 and the subsequent tables.

For rupture and thinning, the response values shown in Table 3 change a few orders of magnitude from minimum to maximum, which can have a negative impact on metamodel accuracy. One way to overcome this challenge is to transform the response values prior to the fitting process. Hence,

Table 2. The design variables and associated properties.

Design variable	Property	Lower bound	Nominal	Upper bound
x_1	Mean width (mm)	40	55	70
x_2	Mean height (mm)	20	27.5	35
x_3	Mean corner radius (mm)	4	6	8
x_4	Mean blank thickness (mm)	1.5	2	2.5
x_5	Mean holding force (kN)	10	30	50
x_6	Mean punch velocity (m/s)	2	6	10
x_7	Mean friction coefficient	0.10	0.225	0.35

Table 3. Bounds of the responses at the random-space training and test points.

Response	Min. at training pts	Max. at training pts	Min. at test pts	Max. at test pts
R	146.5	7966.8	427.4	3401.2
T	0.0956	682.3	14.4	267.0
S (deg.)	0.12	4.57	0.15	2.46
P_{m} (kN)	19.0	107.4	24.6	74.0
$P_{\max}$ (kN)	56.4	229.8	71.1	175.8
M (kg)	0.095	0.334	0.125	0.267

for rupture, thinning and springback, the metamodels are fitted to log 10 of the actual responses. For the other three responses in Table 3, the actual values are used.

The accuracies of the metamodels are evaluated using the root mean square error (RMSE) of the responses at the test points. The RMSE values are normalized with the range (maximum–minimum) of the responses evaluated at the test points. The most accurate (AMM1) and second most accurate (AMM2) metamodel types and their corresponding RMSE values are listed in Table 4. The level of accuracy is very good for most responses and satisfactory for the springback response, which can be more drastically affected as a result of changes in the random variables. It is worth noting that the springback response is highly sensitive to the initial state of stress mapped from the deep-drawing simulation. The small time steps as well as the computational artefacts such as dynamic effects, friction and number of integration points in the explicit solvers introduce noisy results which may cause poor stress distribution and consequently affect the springback response (Xu *et al.* 2004). These factors contribute to the higher-than-average error in the springback metamodels.

Through a Monte Carlo simulation (MCS) framework, the AMM1 of each response is used to sample the space of 12 random variables. Using a sample size of 10,000 with the seven design variables at their nominal values in Table 2, the mean, standard deviation (SD) and coefficient of variation (CoV) of the predicted responses are found to be those given in Table 5. Among all the responses, thinning has the largest CoV as it is affected by geometric and material uncertainty, while mass has the smallest CoV for the nominal case.

Table 4. Error assessment of the analysis metamodels.

			(RMSE/Range) × 100	
Response	AMM1	AMM2	AMM1	AMM2
R	ENS	KR1	4.0	4.6
T	KR1	ENS	5.6	6.7
S	SWR1	KR1	17.8	19.5
P_{m}	ENS	KR1	7.8	7.9
$P_{\max}$	KR1	ENS	2.5	3.2
M	PRS2	ENS	0.5	0.5

Table 5. Random properties of responses with the design variables at their nominal values.

Property	R	T	S (deg.)	P_{m} (kN)	$P_{\max}$ (kN)	M (kg)
Mean	1240.5	84.78	1.690	50.92	126.4	0.1983
SD	169.2	22.52	0.234	1.93	6.07	0.0061
CoV (%)	13.6	26.6	13.8	3.8	4.8	3.1

4.2. *Design metamodels*

The DMMs are constructed to relate the mean and the standard deviation values of the responses to the seven design variables identified in Table 2. The advantage of using DMMs is two-fold: (1) the noise induced by MCS is eliminated; and (2) the solution efficiency is increased.

The DMMs are generated using the same procedure as that for the AMMs except that the training points are in the design-variable space, and uncertainty analysis is performed for each training point using AMM1 found previously for each response. Since the uncertainty analysis is relatively inexpensive with the presence of the AMMs, the number of training points is chosen as 100. The sampling bounds given in Table 2 are used in this analysis. After generating the metamodels, their accuracy is evaluated at 20 test points.

The bounds obtained for the mean and standard deviation values at the design-space training and test points are provided in Tables 6 and 7, respectively.

The prediction accuracy of the DMMs is measured using the RMSE of the responses evaluated at 20 test points. The most accurate (DMM1) and second most accurate (DMM2) metamodel types and their normalized RMSE values are given in Table 8. The metamodels generated for the means and standard deviations of the process and performance responses have acceptable levels of accuracy.

5. Results and discussion

To better explore the influence of underlying uncertainties in material, process and product as defined in Table 1, the results of a sensitivity analysis are presented and discussed first. This is followed by presentation of the solutions to the multi-objective optimization problems in Equations (5)–(7) and their comparison in the context of process–performance optimization under uncertainty.

Table 6. Bounds of the response means at the design-space training and test points.

Response	Min. at training pts	Max. at training pts	Min. at test pts	Max. at test pts
R	359.4	4130.6	517.9	3020.4
T	1.291	900.2	8.139	450.2
S (deg.)	0.280	5.496	0.360	3.817
P_m (kN)	35.7	68.4	40.3	65.8
P_{max} (kN)	71.2	198.2	77.4	168.7
M (kg)	0.112	0.305	0.121	0.258

Table 7. Bounds of the response standard deviations at the design-space training and test points.

Response	Min. at training pts	Max. at training pts	Min. at test pts	Max. at test pts
R	42.7	574.9	66.9	417.5
T	0.650	263.4	3.417	121.3
S (deg.)	0.043	1.122	0.063	0.709
P_m (kN)	1.62	4.26	1.67	4.29
P_{max} (kN)	4.07	7.91	4.83	7.17
M (kg)	0.0046	0.0076	0.0047	0.0074

Table 8. Error assessment of the design metamodels.

			(RMSE/Range) × 100	
Response	DMM1	DMM2	DMM1	DMM2
Metamodels constructed for the mean values of the responses				
R	ENS	KR1	1.0	1.0
T	KR1	ENS	0.9	1.2
S	PRS2	SWR2	0.1	0.1
P_m	ENS	KR1	1.6	1.7
P_{max}	ENS	PRS2	0.6	0.7
M	PRS2	SWR2	0.1	0.1
Metamodels constructed for the standard deviations of the responses				
R	ENS	KR1	3.3	3.4
T	KR1	ENS	1.3	1.3
S	PRS2	SWR2	2.5	2.5
P_m	KR0	ENS	10.8	11.1
P_{max}	KR0	ENS	10.7	11.5
M	PRS1	SWR1	1.5	1.5

5.1. *Sensitivity analysis*

The design variables in Table 2 are normalized in the scale of −1 and +1, and the response values are normalized with the range of response values (*i.e.* the difference between the maximum and the minimum of each response) in the training points. A linear PRS is fitted to the normalized responses in terms of the normalized design variables. The coefficients of the linear terms are treated as the sensitivity of the responses to the design variables. The sensitivity plots are shown in Figures 2–7. In brief, the design variable ID numbers 1–7 refer to the tube width, height, corner radius, blank thickness, holding force, punch velocity and friction coefficient, respectively.

Figure 2 shows that the most important design variable affecting the mean and standard deviation of rupture is the corner radius, which controls the amount of plastic flow in deep drawing. As the corner radius increases, rupture decreases. The coefficients in Figure 2 should be interpreted as follows. For example, if the corner radius is increased by 10% from its nominal value, rupture will reduce by 0.02 times the range of response values at the training points (see Table 6 for the range). Figures 2 and 3 show that the sensitivities of rupture and thinning are fairly similar.

Figure 4 shows that the most influential design variables for the mean and standard deviation of springback are the height, corner radius and blank thickness, as they affect strongly the stress distribution state in the tube. The mean springback as well as its variance can be reduced by decreasing the height and the corner radius and by increasing the thickness. Decreasing the

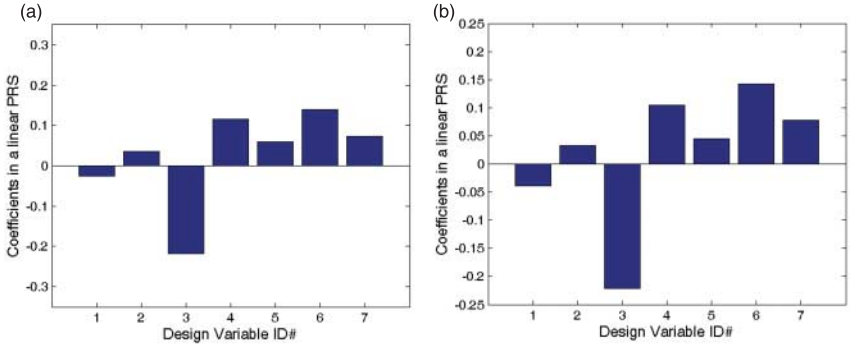

Figure 2. Sensitivities of the rupture (R) statistical properties to design variables.

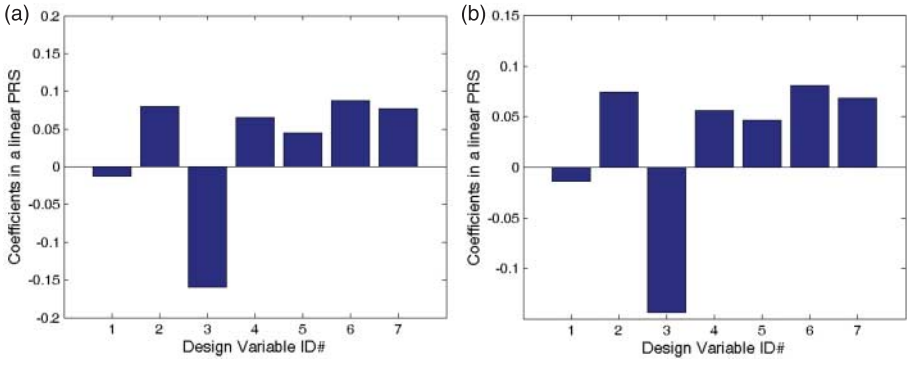

Figure 3. Sensitivities of the thinning (T) statistical properties to design variables.

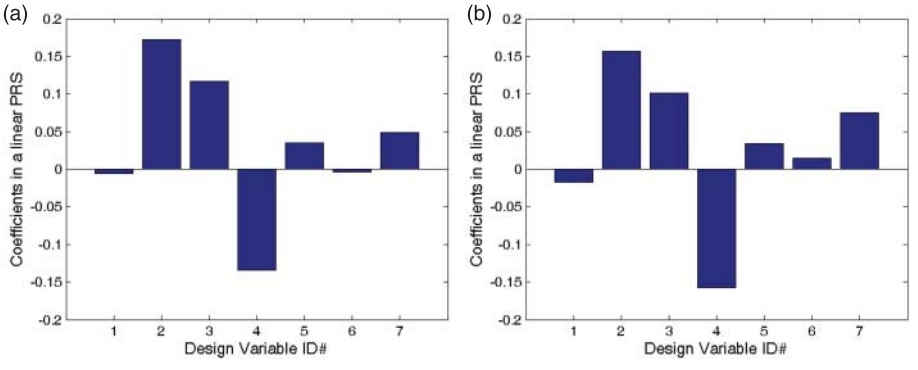

Figure 4. Sensitivities of the springback (S) statistical properties to design variables.

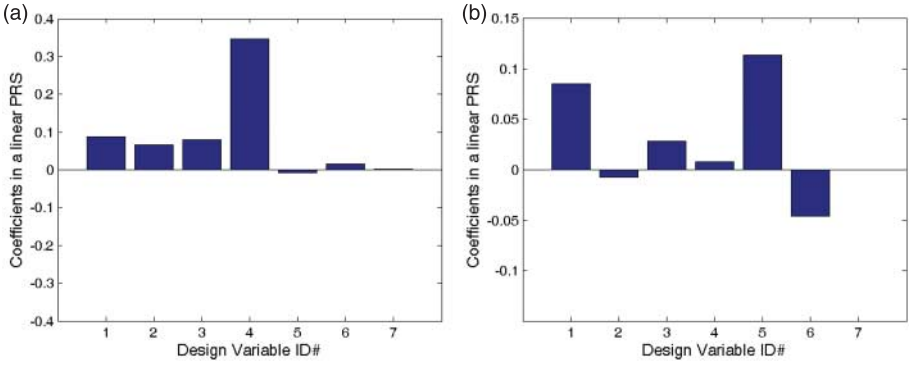

Figure 5. Sensitivities of the mean crush force (P_{m}) statistical properties to design variables.

height reduces the stress-affected plastic zones in the material. As the corner radius decreases, the localized plastic deformation becomes more confined to the corner regions. The increase in blank thickness also reduces the amount of springback due to increase in plastic deformation through the tube wall.

Figures 5–7 show that the sensitivities of the mean crush force, the maximum crush force and mass are fairly similar. Since mass is not a function of the manufacturing process parameters, the plots in Figure 5 only show the influence of design variables 1–4. The most significant design

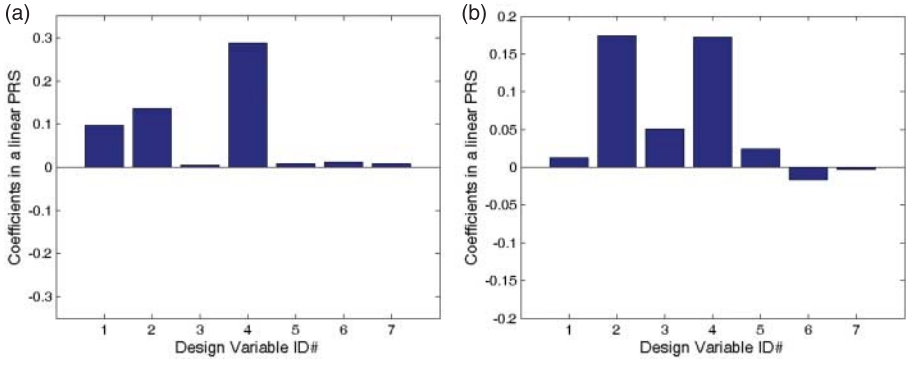

Figure 6. Sensitivities of the maximum crush force (P_{max}) statistical properties to design variables.

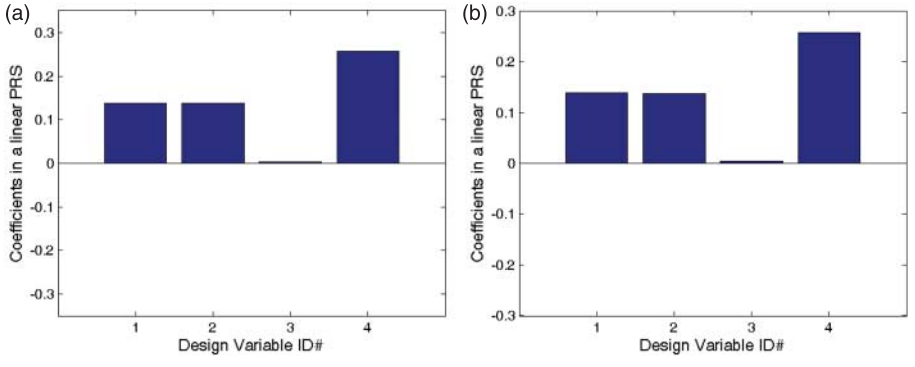

Figure 7. Sensitivities of the mass (M) statistical properties to design variables.

variable for these responses is found to be the thickness. If it is increased, all of these responses increase significantly. This is not surprising as thickness has a significant influence on the energy absorption and mass of thin-walled tubes.

Although for the manufacturing responses the approach used here provides reasonable estimates of the relative importance of each design variable, for the performance responses, a more accurate procedure would involve the use of global sensitivity equations (Sobieszczanski-Sobieski 1990).

5.2. *Robust multi-objective optimization*

The multi-objective robust optimization problem in Equation (5) was solved by using the built-in function '*gamultiobj*' of MATLAB Global Optimization Toolbox, which is an implementation of the multi-objective genetic algorithm (MOGA) (Fonseca and Fleming 1993; MATLAB 2012).

For this problem, the optimizer was able to find 37 points on the six-dimensional Pareto frontier, as listed in Table 9. If the Pareto set is sorted from the best to worst for each objective, the order for the top five best designs in each category would be that shown in Table 10. For example, the best design for rupture and thinning appears to be the one at Pareto point 11, with 22 being the best for springback, 3 for the mean crush force, 5 for the maximum crush force, and 2 for mass. In about 25% of the Pareto points in Table 9, a match is seen between rupture and thinning. This is reasonable considering the sensitivity charts in Figures 2 and 3. However, there is very little agreement in the other cases, which is to be expected in a multi-objective optimization problem.

Table 9. Reduced set of design points on the Pareto frontier of the robust design problem.

Pareto point	Width (mm)	Height (mm)	Corner radius (mm)	Blank thickness (mm)	Holding force (kN)	Punch velocity (m/s)	Friction coeff.	SD					
								R	T	S (deg.)	P_m (kN)	P_{max} (kN)	M (kg)
1	49.6	21.6	4.36	2.49	50.0	9.29	0.127	521.6	84.1	0.044	1.95	5.61	0.0052
2	40.8	20.3	6.77	1.61	41.7	4.76	0.330	123.8	13.0	0.335	1.75	4.56	0.0046
3	63.7	22.0	6.29	2.37	30.7	7.62	0.236	195.6	24.4	0.142	1.31	5.20	0.0060
4	68.4	32.5	7.18	2.33	30.5	3.82	0.157	96.5	8.9	0.264	1.67	7.61	0.0074
5	62.0	21.4	4.16	1.62	17.8	3.83	0.334	183.6	25.8	0.122	2.25	3.97	0.0058
6	67.3	22.8	6.91	1.92	49.5	3.78	0.142	83.9	5.4	0.240	4.31	5.81	0.0063
7	69.4	34.3	7.03	2.03	28.0	7.33	0.121	114.6	14.3	0.360	1.53	6.99	0.0076
8	44.8	22.0	4.34	2.43	48.4	9.57	0.221	639.4	132.4	0.053	1.87	5.86	0.0050
9	68.3	20.7	4.27	2.39	49.7	9.69	0.319	591.3	173.6	0.046	2.76	5.39	0.0061
10	47.5	20.7	4.38	2.38	43.5	9.39	0.257	592.5	113.9	0.060	1.82	5.68	0.0050
11	68.3	22.9	7.95	1.54	24.5	3.40	0.124	35.9	0.7	0.508	2.36	5.34	0.0063
12	66.1	33.1	7.05	1.59	23.0	6.37	0.257	101.6	14.9	0.682	1.57	6.14	0.0073
13	68.5	25.3	6.62	1.91	49.8	3.83	0.166	96.8	8.3	0.228	4.61	6.09	0.0066
14	58.7	22.4	4.27	1.81	20.7	7.44	0.299	300.0	46.8	0.130	2.02	4.43	0.0058
15	68.3	22.5	4.27	2.39	49.7	8.82	0.194	441.5	98.8	0.049	3.04	5.28	0.0063
16	64.5	22.1	5.51	2.38	34.1	7.72	0.259	263.9	43.1	0.106	1.46	5.14	0.0061
17	68.4	31.2	7.20	1.79	31.9	6.23	0.189	88.9	12.0	0.439	1.71	6.42	0.0072
18	45.0	22.3	4.33	2.08	27.5	7.59	0.282	410.3	59.7	0.102	2.15	5.40	0.0050
19	43.3	22.1	4.33	2.44	48.1	8.96	0.299	708.6	179.2	0.071	1.99	6.10	0.0050
20	63.3	22.8	4.85	2.17	48.5	6.27	0.174	254.0	34.1	0.090	3.25	5.54	0.0061
21	64.5	20.7	4.27	2.39	49.7	9.69	0.319	617.8	177.8	0.050	2.62	5.44	0.0059
22	68.3	20.7	4.27	2.39	49.7	9.69	0.287	558.4	152.4	0.043	2.77	5.30	0.0061
23	69.9	34.8	7.05	1.61	28.0	6.62	0.257	103.6	18.9	0.716	1.48	6.28	0.0076
24	58.7	22.4	4.27	1.94	20.7	8.44	0.299	363.6	61.5	0.114	2.01	4.60	0.0058
25	67.5	31.9	7.18	2.33	40.4	5.16	0.151	115.5	12.5	0.258	2.63	7.69	0.0073
26	65.8	23.5	4.82	2.29	49.8	6.62	0.234	318.4	53.8	0.080	3.49	5.67	0.0063
27	63.9	22.6	7.31	1.72	23.1	3.57	0.258	62.5	2.8	0.313	2.17	5.10	0.0061
28	64.3	21.4	4.65	2.27	49.4	6.83	0.228	331.8	52.2	0.067	3.11	5.37	0.0060
29	63.7	20.7	4.35	2.44	50.0	9.41	0.272	565.8	141.0	0.047	2.62	5.34	0.0059
30	63.7	21.9	4.17	2.04	44.5	4.07	0.332	288.3	48.5	0.086	2.92	5.47	0.0060
31	63.9	29.9	7.21	1.77	29.5	6.43	0.324	117.2	21.4	0.559	1.81	6.07	0.0068
32	57.5	21.7	4.57	2.48	49.8	7.94	0.192	443.3	76.2	0.056	2.44	5.46	0.0057
33	62.6	21.6	4.24	1.73	26.1	3.99	0.305	186.6	28.4	0.119	2.05	4.26	0.0059
34	64.2	22.3	4.79	2.36	49.3	7.27	0.289	395.5	77.4	0.075	3.03	5.55	0.0061
35	52.3	22.2	4.34	2.22	30.7	7.70	0.278	420.8	70.1	0.090	1.77	5.36	0.0054
36	68.3	26.7	7.95	1.79	34.5	2.90	0.124	44.2	1.7	0.472	2.43	6.05	0.0067
37	68.3	22.5	4.27	2.39	49.7	8.82	0.256	494.8	127.8	0.050	2.97	5.36	0.0063

Table 10. Sorted listing of design points on the Pareto frontier of the robust design problem.

R	T	S	P_m	P_{max}	M
11	11	22	3	5	2
36	36	1	16	33	19
27	27	9	23	14	8
6	6	29	7	2	10
17	13	15	12	24	18

Generally speaking, reducing variability in one response does not guarantee a similar trend in the others. A clear trade-off exists in enhancing robustness among the responses of interest against the underlying uncertainties in the process–product system.

A closer look at the values of product design variables in Table 9 shows that in order to minimize the variance in the selected responses, the majority of cases (30/37 or 81%) call for an optimum tube with width being larger than the nominal value in Table 2. Consistent with this trend is the fact that in only seven Pareto design points we see the tube height exceed its nominal value. For corner radius, 24 design points have values smaller than the nominal, and 23 design points have thickness larger than the nominal value.

It appears that, in general, a wide and short rectangular cross-section is preferred to a narrow and tall or a square cross-section in robust optimum designs; furthermore, it is preferable to have a small corner radius and a large blank thickness. The preference for dissimilar width and height dimensions under axial crush conditions can be traced to several factors. Most notable is the fact that the entire tube wall along the height portion undergoes plastic deformation during the forming process; therefore, there is more strain hardening in the vertical than in the horizontal walls. In addition, because of the flanges in the double-hat geometry (see Figure 1), the height and width sections of the tube undergo different amounts of deformation and contribute differently to the crush energy absorption.

As far as the process design variables are concerned, Table 9 shows that it is preferable for the holding force to be larger than its nominal value in 26/37 (70%) of the Pareto set. A nearly equal percentage of the design set prefers a higher punch velocity and a lower friction coefficient than the respective nominal values. These results appear, at first glance, to contradict the sensitivity results. However, what they actually reveal is the presence of interaction among the design variables, which is not captured by the main effects presented in the sensitivity plots.

5.3. *Deterministic multi-objective optimization*

The deterministic optimization problem in Equation (6) was also solved using the MATLAB MOGA toolbox with an initial population size of 105 (15 times the number of design variables). The initial population was created by using a random number generator in MATLAB within the bounds of the design variables in Table 2. The tournament selection algorithm was used for identifying the parents for forming the subsequent generations. The crossover fraction was selected as 80% using the intermediate crossover function, and the function tolerance to stop the optimization procedure was set to 10^{-4}. The stopping criterion was applied at generation number 100.

In this problem, the optimizer found 41 non-dominated design points on the Pareto frontier, as shown in Table 11. As expected from a Pareto optimal set, no design point can be found where all the objective functions simultaneously reach their respective optimum values. However, by sorting the Pareto set from the best to worst design for each objective, the order for the top five best designs in each category as well as the degree of conflict among them can be found in Table 12.

Table 11. Reduced set of design points on the Pareto frontier of the deterministic design problem.

Pareto point	Width (mm)	Height (mm)	Corner radius (mm)	Blank thickness (mm)	Holding force (kN)	Punch velocity (m/s)	Friction coeff.	Mean value					
								R	T	S (deg.)	P_m (kN)	P_{max} (kN)	M (kg)
1	42.7	25.0	4.67	1.62	32.6	2.49	0.270	1145.4	88.2	1.09	37.4	87.4	0.135
2	66.9	21.9	4.16	2.50	22.8	9.09	0.306	3856.6	528.7	0.22	60.6	162.0	0.248
3	47.7	29.0	7.94	1.66	10.6	2.61	0.110	321.2	2.7	1.83	45.7	98.7	0.159
4	41.6	23.1	5.33	1.59	27.1	2.23	0.226	785.2	38.7	0.87	36.8	80.3	0.126
5	53.0	33.0	7.44	1.75	28.9	6.04	0.279	792.2	59.6	4.32	49.0	120.3	0.188
6	61.9	33.2	4.55	2.47	29.2	8.41	0.307	3861.7	743.2	1.10	64.1	187.6	0.285
7	58.0	28.5	4.48	2.24	41.4	8.79	0.299	3654.6	548.7	0.93	56.1	152.6	0.231
8	53.9	33.5	7.63	1.74	35.0	6.65	0.331	928.0	98.5	5.31	49.6	123.2	0.191
9	56.3	33.7	7.74	1.66	27.6	5.67	0.279	657.6	42.2	4.92	48.2	117.1	0.185
10	46.0	26.5	4.48	1.61	30.6	3.77	0.253	1282.5	110.9	1.46	37.9	91.6	0.143
11	67.6	34.1	7.29	2.50	17.3	8.72	0.307	1729.0	167.9	1.71	70.7	198.6	0.306
12	58.8	30.9	4.35	2.48	39.1	9.13	0.312	4723.7	988.4	0.85	62.5	179.4	0.269
13	60.0	27.5	4.57	1.68	26.6	8.14	0.285	1994.8	217.7	1.58	43.6	110.1	0.174
14	55.4	34.4	7.73	1.74	32.5	6.65	0.339	897.7	94.7	5.79	50.4	126.4	0.196
15	57.4	33.3	7.15	1.74	32.4	6.32	0.312	956.8	100.0	4.63	49.6	124.5	0.195
16	54.1	32.5	5.58	2.15	40.2	8.74	0.324	2757.5	412.3	2.32	56.3	154.6	0.231
17	66.6	34.1	7.02	2.47	18.8	8.71	0.318	1885.1	201.8	1.76	69.5	195.6	0.301
18	66.9	32.0	4.18	2.50	40.7	9.41	0.319	5020.6	1310.3	0.62	64.7	190.9	0.293
19	41.3	22.9	5.44	1.56	27.9	2.22	0.226	750.3	34.7	0.90	36.2	77.9	0.123
20	55.6	29.0	5.04	2.23	28.2	8.70	0.310	2865.6	364.8	1.29	56.5	150.9	0.228
21	52.2	30.6	5.88	1.74	34.0	7.97	0.297	1577.1	173.8	3.10	46.2	115.1	0.178
22	52.8	34.2	7.54	1.74	31.4	5.72	0.303	803.2	70.3	5.07	49.1	122.7	0.191
23	49.7	29.3	7.87	1.69	19.3	6.26	0.285	628.9	26.2	3.29	47.3	105.9	0.166
24	52.8	33.9	6.94	2.03	38.5	7.63	0.321	1536.8	191.1	3.80	55.3	147.4	0.222
25	58.1	30.6	4.36	2.48	39.6	9.55	0.313	4936.5	1053.6	0.83	62.3	178.1	0.266
26	62.7	27.4	5.89	2.07	42.2	9.46	0.327	2301.9	295.7	1.24	54.7	142.1	0.219
27	43.5	24.3	5.48	1.73	29.0	5.83	0.264	1227.1	85.9	1.29	41.3	94.1	0.143
28	67.7	32.0	4.18	2.50	43.2	9.41	0.319	5105.6	1365.6	0.57	65.1	191.7	0.295
29	46.8	28.5	7.91	1.71	24.5	2.77	0.311	488.1	13.9	2.89	45.7	102.8	0.161
30	58.6	31.8	5.10	2.16	35.1	8.33	0.309	2735.3	394.9	1.79	56.2	155.6	0.237
31	64.6	33.7	6.75	2.50	27.6	8.88	0.320	2125.8	273.3	1.78	68.4	195.5	0.297
32	61.0	23.2	4.29	2.50	35.7	9.12	0.311	4172.8	605.4	0.35	59.7	160.2	0.240
33	61.9	30.0	6.23	2.36	41.8	9.40	0.322	2554.5	348.4	1.36	62.6	171.9	0.259
34	54.7	30.6	6.87	2.01	29.6	3.72	0.237	816.0	40.1	2.49	53.1	135.4	0.211

(*Continued*)

Table 11. Continued

Pareto point	Width (mm)	Height (mm)	Corner radius (mm)	Blank thickness (mm)	Holding force (kN)	Punch velocity (m/s)	Friction coeff.	Mean value					
								R	T	S (deg.)	P_m (kN)	P_{max} (kN)	M (kg)
35	61.2	25.6	5.57	2.37	34.4	8.17	0.331	2516.0	283.7	0.92	59.3	158.5	0.240
36	51.4	28.5	6.33	2.11	24.6	7.85	0.307	1607.7	146.4	1.98	54.8	136.5	0.206
37	67.0	34.1	5.43	2.50	34.8	8.87	0.320	3199.9	588.0	1.16	66.9	198.0	0.304
38	60.1	28.0	4.57	1.70	26.9	8.15	0.290	2048.9	230.3	1.66	44.1	112.1	0.177
39	58.8	30.9	4.35	2.48	39.1	9.13	0.320	4789.9	1025.8	0.87	62.5	179.5	0.269
40	58.9	30.6	4.36	2.48	40.9	9.55	0.321	5035.6	1113.6	0.81	62.6	178.9	0.268
41	65.1	28.2	4.47	2.50	44.0	9.61	0.312	4631.0	905.8	0.46	63.5	179.2	0.272

Table 12. Sorted listing of design points on the Pareto frontier of the deterministic design problem.

R	T	S	P_m	P_{max}	M
3	3	2	11	19	19
29	29	32	17	4	4
23	23	41	31	1	1
9	19	28	37	10	10
19	4	18	28	27	27

For example, the best design for rupture and thinning is the Pareto point 3; for the maximum crush force and mass, the best design is at Pareto point 19, with 2 being the best for springback and 11 for the mean crush force.

It appears that rupture and springback are in strong competition with each other as well as the other objectives, whereas rupture and thinning are in agreement in approximately 37% of the Pareto set. While large plastic deformation tends to reduce springback, it can increase the amount of thinning or the likelihood of rupture. Hence, the trend observed is supported by the physics of the problem.

The maximum crush force and mass are found to be in agreement in approximately 80% of the Pareto set. That is, an optimal design for maximum crush force is mostly an optimum design for mass. Since the maximum crush force is generally associated with excessive stiffness in the tube, an effective way to reduce it would be through reduction of cross-sectional size or wall thickness, both of which tend to also reduce the mass. However, the same relationship is not seen between mass and the mean crush force; this is because unlike the maximum crush force, it is desirable to increase the mean crush force as much as possible since that would enhance the energy absorption capacity of the tube.

By examining the optimal values of product design variables in Table 11, it can be seen that among the Pareto optimal designs, approximately 61% prefer a larger width, 76% a larger height, 61% a smaller corner radius and 59% a larger blank thickness than their respective nominal values. Unlike in the previous case, the goal of this optimization problem is to enhance the overall performance and manufacturability of the tube assuming no variability in the design. Here, the preferred geometry is more towards a design with longer height than width. As for the process design variables, a greater holding force (∼56%), a higher punch velocity (∼76%) and a larger friction coefficient (∼98%) than nominal are preferred among the Pareto optimum design points.

5.4. *Augmented robust optimum design*

The solution to the multi-objective optimization problem in Equation (7) resulted in 50 Pareto optimal design points. The metamodels used for the mean values are those generated for the deterministic optimum design problem, whereas those for the variances are those developed for

Table 13. Sorted listing of design points on the Pareto frontier of the augmented robust design problem.

Mean value						Variance					
R	T	S	P_m	P_{max}	M	R	T	S	P_m	P_{max}	M
12	3	1	24	23	23	12	3	1	49	6	2
3	12	43	4	14	2	3	12	43	40	23	23
37	37	36	50	2	14	37	37	36	22	14	14
28	11	41	10	6	6	28	11	14	43	2	6
11	28	35	40	31	31	11	28	35	31	1	43

Table 14. A subset of design points on the Pareto frontier of the augmented robust design problem.

Pareto point	Width (mm)	Height (mm)	Corner radius (mm)	Blank thickness (mm)	Holding force (kN)	Punch velocity (m/s)	Friction coeff.	Mean value (SD)					
								R	T	S (deg.)	P_m (kN)	P_{max} (kN)	M (g)
1	70.0	22.9	4.00	2.50	10.0	10.0	0.116	3306 (417)	288 (67)	0.16 (0.04)	62.9 (2.5)	164.6 (4.8)	259.6 (6.4)
2	41.8	20.9	4.89	1.59	27.5	7.5	0.340	1690 (266)	140 (35)	1.02 (0.22)	36.7 (2.1)	79.4 (4.5)	119.8 (4.7)
3	68.6	27.2	7.50	1.59	18.4	3.3	0.117	369 (45)	2.5 (1)	2.59 (0.46)	46.5 (2.3)	105.8 (5.7)	177.5 (6.8)
4	69.9	34.6	6.21	2.50	40.9	9.8	0.325	2871 (376)	537 (138)	1.11 (0.23)	69 (2.2)	202.9 (7.2)	313.2 (7.7)
6	51.4	21.1	5.00	1.58	17.2	4.9	0.316	1129 (162)	66 (18)	0.96 (0.17)	38.9 (2.1)	85.1 (4.1)	133 (5.2)
10	67.2	34.0	5.93	2.49	44.2	4.3	0.154	1462 (189)	125 (31)	1.28 (0.17)	68.1 (3.1)	195.3 (8)	302.7 (7.5)
11	69.4	27.3	6.56	2.03	49.9	2.7	0.158	790 (97)	27 (8)	1.43 (0.22)	57.6 (4.7)	142.5 (6.7)	226.9 (6.9)
12	69.5	27.7	7.63	1.61	19.7	3.2	0.118	357 (43)	2.5 (1)	2.7 (0.48)	47.1 (2.3)	108.5 (5.8)	181.8 (6.9)
14	43.4	21.7	4.10	1.56	33.2	4.3	0.215	1363 (191)	99 (23)	0.74 (0.14)	34.8 (2)	78 (4.4)	121.3 (4.9)
22	59.2	34.0	6.13	1.59	33.3	7.5	0.238	1135 (154)	112 (30)	4.24 (0.78)	45.5 (1.8)	115.3 (5.9)	182 (7)
23	42.8	21.2	4.60	1.56	30.4	4.0	0.257	1179 (167)	80 (19)	0.8 (0.15)	35.1 (2.1)	77 (4.3)	119.6 (4.8)
24	69.4	34.6	6.74	2.50	14.7	10.0	0.341	2427 (312)	303 (71)	1.35 (0.28)	71.2 (2.2)	201.1 (6.8)	312.1 (7.6)
28	68.1	27.6	6.76	1.74	45.1	2.9	0.232	669 (82)	27 (9)	2.04 (0.32)	50 (4)	119.8 (6)	193.5 (6.8)
31	47.6	26.9	4.12	1.56	45.0	7.7	0.200	2177 (293)	196 (51)	1.51 (0.27)	37.9 (1.8)	92.4 (5.2)	142.1 (5.6)
35	64.7	33.0	4.30	2.41	46.7	9.4	0.255	4472 (607)	981 (282)	0.73 (0.14)	63.5 (2.8)	184.8 (7.2)	282.6 (7.2)
36	64.2	30.7	4.09	2.46	46.4	9.9	0.256	5037 (678)	1114 (316)	0.5 (0.1)	63.2 (2.7)	181.7 (6.8)	276.8 (6.9)
37	68.5	27.6	7.21	1.69	42.0	3.2	0.128	477 (57)	10 (4)	2.51 (0.42)	49.1 (3.3)	115.6 (5.9)	189.3 (6.8)
40	67.9	34.3	5.02	2.50	28.7	9.7	0.320	3869 (502)	787 (210)	0.97 (0.21)	67.2 (1.8)	198.9 (6.9)	306.6 (7.5)
41	61.0	30.7	4.16	2.47	47.0	9.8	0.335	5864 (784)	1569 (442)	0.68 (0.15)	62.8 (2.5)	180 (6.6)	271 (6.8)
43	50.6	21.6	4.31	2.35	42.1	8.6	0.323	4120 (586)	498 (137)	0.45 (0.08)	55 (1.8)	135.5 (5.8)	198.2 (5.3)
49	67.4	33.3	4.57	1.67	26.5	7.3	0.323	2008 (271)	271 (69)	2.76 (0.6)	46.6 (1.3)	126.3 (6.2)	200.5 (7.3)
50	69.9	34.6	6.21	2.50	40.9	9.7	0.327	2872 (376)	538 (139)	1.11 (0.24)	69 (2.2)	202.9 (7.2)	313.2 (7.7)

the robust design problem. The sorted order of the top five best designs in each category is shown in Table 13. Repeated numbers in each row identify the degree of agreement among the design points in the Pareto set. The corresponding design variable values as well as the mean and standard deviation of each response are shown in Table 14.

In terms of geometry, the general preference is for a tube with larger height than width. On average, the tube width and height values for the Pareto optimum designs in this case are larger than those for the deterministic optimum designs.

For thinning, it appears that in the majority of cases (31/50 or 62%), a design that minimizes the mean value of thinning also minimizes the corresponding variance. For the remaining five responses, the level of agreement between a design that minimizes the mean and the one that minimizes the variance is found to be 54% for rupture, 26% for springback, 0% for the mean crush force, 4% for the maximum crush force and 14% for the tube mass. Although there appears to be considerable agreement between the Pareto points that optimize the mean value of a process response and those that minimize the corresponding variance, the same trend cannot be seen among the performance responses.

Comparison of Pareto optimum designs here with the deterministic optimum designs shows a wider spread in the responses among the Pareto points due to the presence of random variability. For example, the range for the mean rupture response is 6591 or approximately 2 SD greater than the range of 4784 in the deterministic case. Similarly, for the mean thinning, the range is 2340 or 1.5 SD greater than the thinning range of 1363 in the deterministic case.

6. Concluding remarks

A finite element-based sequential coupled process–performance simulation framework was used to explore the effect of uncertainties rooted in process, material and product parameters on manufacturability and performance characteristics of energy-absorbing components. The manufacturing method considered was thin sheet forming using a deep-drawing operation with rupture, thinning and springback as the manufacturability metrics of interest. With a thin-walled, double-hat crush tube as an example, separate metamodels were developed for uncertainty propagation and approximation of process and performance responses in the design space.

The sensitivity analysis results showed that, in the presence of uncertainty, the most important design variable affecting the mean and standard deviation of rupture and thinning is the corner radius, whereas for springback, tube height and blank thickness have the greatest influence, with corner radius close behind. Rupture and thinning generally show similar preference for each of the seven design variables, which is different from springback, hence pointing to the presence of conflict among the manufacturing response parameters. As for the performance responses, the trends for the maximum crush force and tube mass are very similar as both are driven by the geometric properties of the tube and are strongly dependent on blank thickness. Although the mean and maximum crush forces show the same general trend when it comes to sensitivity of the mean response, they show a strong contrast in terms of variance sensitivity. In general, the variability observed in all the process and performance responses highlights the strong influence of the underlying uncertainties in the process–product system.

With the goal of minimizing the variance of process and performance objectives due to the embedded uncertainties, a robust multi-objective design optimization problem was formulated and solved. The results indicated that a robust design generally requires a crush tube with a wide and short rectangular cross-section, small corner radius and large blank thickness. These requirements were accompanied by a general preference for a greater holding force, higher punch velocity and smaller friction coefficient than the nominal values in the sheet-forming process.

When the focus shifted to optimizing the process and performance responses by ignoring the existence of uncertainties and the risk associated with them, a deterministic Pareto optimal set was found. Although the objectives were in competition, there was a strong preference for a tube with a larger width and height, smaller corner radius and larger blank thickness than their respective nominal values. The main difference with the robust Pareto set was the opposite demand for a larger height and higher friction coefficient.

By combining the robust and deterministic design problems, a larger multi-objective optimization problem was formulated and solved with equal emphasis on optimizing the mean values of the responses while minimizing the corresponding variances. The results showed that there was moderate to significant agreement among the designs with the mean and variance of the manufacturing responses optimized, whereas there was minimal to no agreement among the designs with the mean and variance of the performance responses optimized. In addition, the range of values for each mean response among the Pareto set was greater in the augmented robust design case than in the deterministic case. This difference indicates that the inclusion of uncertainties yields a more conservative Pareto set.

Acknowledgements

Partial funding for this project provided by the US Department of Energy under award number DE-EE0002323 is gratefully acknowledged.

References

Abaqus/Explicit version 6.10, User's Manual. 2010. Pawtucket, RI: Hibbit, Karlsson and Sorensen.

Abaqus/Standard version 6.10, User's Manual. 2010. Pawtucket, RI: Hibbit, Karlsson and Sorensen.

Acar, E. and M. Rais-Rohani. 2008. "Ensemble of Metamodels with Optimized Weight Factors." *Structural and Multidisciplinary Optimization*, 37 (3), 279–294.

Buhmann, M. 2003. *Radial Basis Functions: Theory and Implementations*. New York: Cambridge University Press.

Dutton, T., R. Sturt, P. Richardson, and A. Knight. 2001. *The Effect of Forming on Automotive Crash Results*. SAE Paper, 2001-01-3050.

Fonseca, M., and P. J. Fleming. 1993. "Genetic Algorithms for Multiobjective Optimization: Formulation, Discussion and Generalization." In *Proceedings of the 5th International Conference on Genetic Algorithms*. San Francisco: Morgan Kaufmann, 416–423.

Gholipour, J., M. Worswick, and D. Oliveira. 2004. *Application of Damage Models in Bending and Hydroforming of Aluminum Alloy Tube*. SAE Technical Paper 2004-01-0835.

Grantab, R., 2006. "*Interaction between Forming and Crashworthiness of Advanced High Strength Steel S-Rails*." PhD dissertation, University of Waterloo, Canada.

Hu, W., L. Yao, and Z. Hua. 2008. "Optimization of Sheet Metal Forming Processes by Adaptive Response Surface Based on Intelligent Sampling Method." *Journal of Materials Processing Technology*, 197 (1–3), 77–88.

Kaufman, M., D. Gaines, K. Kundrick, and S. Liu. 1998. *Integration of Chassis Frame Forming Analysis into Performance Models to More Accurately Evaluate Crashworthiness*. SAE Technical Paper 980551.

Lee, S., Y. N. Kwon, S. H. Kang, S. W. Kim, and J. H. Lee. 2008. "Forming limit of AZ31 Alloy Sheet and Strain Rate on Warm Sheet Metal Forming." *Journal of Materials Processing Technology*, 201 (1–3), 431–435.

Martin, J., and T. Simpson. 2005. "Use of Kriging Models to Approximate Deterministic Computer Models." *AIAA Journal*, 43 (4), 853–863.

MATLAB Global Optimization Toolbox R2012b. 2012. The MathWorks, Inc.

Mullur, A. A., and A. Messac. 2005. "Extended Radial Basis Functions: More Flexible and Effective Metamodeling." *AIAA Journal*, 43 (6), 1306–1315.

Myers, R., and D. Montgomery. 2002. *Response Surface Methodology: Process and Product Optimization Using Designed Experiments*. New York: Wiley.

Najafi, A., and M. Rais-Rohani. 2012. "Sequential coupled process-performance simulation and multi-objective optimization of thin-walled tubes." *Materials and Design*, 41, 89–98.

Najafi, A., and M. Rais-Rohani. 2011. "Mechanics of Axial Plastic Collapse in Multi-Cell, Multi-Corner Crush Tubes." *Thin-Walled Structures*, 49, 1–12.

Najafi, A., E. Marin, and M. Rais-Rohani. 2012. "Concurrent Multi-Scale Crush Simulations with a Crystal Plasticity Model." *Thin-Walled Structures*, 53, 176–187.

Najafi, A., M. Rais-Rohani, and Y. Hammi. 2011. "Multi-Attribute Integrated Forming-Crush Simulation Optimization Using Internal State Variable Model." In *Proceedings of the 1st World Congress on Integrated Computational Materials Engineering*, Seven Springs, PA, TMS. July, pp. 1–14.

Oliveira, D., M. Worswick, R. Grantab, B. Williams, and R. Mayer. 2006. "Effect of Forming Process Variables on the Crashworthiness of Aluminium Alloy Tubes." *International Journal of Impact Engineering*, 32 (5), 826–846.

Qu, X., R. Haftka, S. Venkataraman, and T. Johnson. 2003. "Deterministic and Reliability-Based Optimization of Composite Laminates for Cryogenic Environments." *AIAA Journal*, 41 (10), 2029–2036.

Sacks, J., W. Welch, T. Mitchell, and H. Wynn. 1989. "Design and Analysis of Computer Experiments." *Statistical Sciences*, 4 (4), 409–435.

Simunovic, S., and G. Aramayo. 2002. *Steel Processing Properties and Their Effect on Impact Deformation of Lightweight Structures*. Computer Science and Mathematics Division, Computational Materials Science Group, American Iron and Steel Institute.

Simunovic, S., J. Shaw, and G. Aramayo. 2001. *Steel Processing Effects on Impact Deformation of UltraLight Steel Auto Body*. SAE Technical Paper 2001-01-1056.

Sobieszczanski-Sobieski, J. 1990. "Sensitivity Analysis and Multidisciplinary Optimization for Aircraft Design: Recent Advances and Results." *Journal of Aircraft*, 27 (12), 993–1001.

Wei, L., and Y. Yuying. 2008. "Multi-objective Optimization of Sheet Metal Forming Process Using Pareto-Based Genetic Algorithm." *Journal of Materials Processing Technology*, 208 (1–3), 499–506.

Williams, B., D. Oliveira, M. Worswick, R. Mayer. 2005. *Crashworthiness of High and Low Pressure Hydroformed Straight Section Aluminum Tubes.* SAE Technical Paper 2005-01-0095.

Xu, X., C. Ma, C. Li, W. Feng. 2004. "Sensitive Factors in Springback Simulation for Sheet Metal Forming." *Journal of Materials Processing Technology*, 151, 217–222.